Est. 1984

ORIENTAL JOURNAL OF CHEMISTRY
An International Open Free Access, Peer Reviewed Research Journal

www.orientjchem.org

ISSN: 0970-020 X
CODEN: OJCHEG
2015, Vol. 31, No. (3):
Pg. 1537-1544

Application of Porphyrin Modified SBA-15 in Adsorption of Lead Ions from Aqueous Media

MOHAMMAD SADEGH ASGARI[1]*, AFSANEH ZONOUZI[1], RAHMATOLLAH RAHIMI[2] and MAHBOUBEH RABBANI[2]

[1]Department of Chemistry, University of Tehran, Enghelab, Tehran, Iran
[2]Department of Chemistry, Iran University of Science and Technology, Narmak, Tehran, Iran
*Corresponding author E-mail: Sadeghasgari1@gmail.com

http://dx.doi.org/10.13005/ojc/310331

(Received: July 13, 2015; Accepted: August 14, 2015)

ABSTRACT

Mesoporous silica SBA-15 was synthesized using P123 as surfactant and functionalized with (3-chloropropyl) triethoxysilane. For the first time, the composite of THPP-SBA-15 was prepared using incorporation of tetrakis(4-hydroxyphenyl)porphyrin in functionalized SBA-15. The materials were characterized by BET, SEM, XRD, FT-IR, DRS, and UV–Vis spectroscopy techniques. The synthesized composite was employed as adsorbent of heavy metal ion (Pb^{2+}) from water at room temperature. Results indicated that the presence of porphyrin in silica significantly increased heavy metal ion adsorption. The maximum adsorption capacity (q_{max}) of THPP-SBA-15 for Pb^{2+} was found to be 134 mg/g.

Key words: SBA-15, Tetrakis(4-hydroxyphenyl)porphyrin, THPP, Lead, Adsorption.

INTRODUCTION

Mesoporous silica materials have attracted considerable attention as support for different molecules, because these materials possess high surface area, large uniform pores, photostability, rigidity, and diverse surface properties by various types of modifiers[1-3]. Among mesoporous silica materials, the Santa Barbara Amorphous (SBA-15) has large pore size (from 3 to 30 nm), high surface area, and high hydrothermal and thermal stability[4-8]. The greater wall thickness of SBA-15 compared to materials like MCM-41 can be considered an important advantage for this material[9,10]. The SBA-15 is prepared by interaction of tetraethoxysilane (TEOS), and a Pluronic P123 tri-block copolymer ($EO_{20}PO_{70}EO_{20}$, MW. 5800), as a template[6]. At low pH, the EO units (hydrophilic head-groups) and the silica species (positively charged) are assembled together through electrostatic interactions by anions (negatively charged)[9,10].

Many studies have been carried out recently on designing and preparing the organic–inorganic hybrid of SBA-15 by functionalization of their wall surface with organic groups for different applications[2,11,29,30], such as catalysts[12], enzyme carriers[13], and adsorbents for removal of toxic heavy metal ions from wastewater[14-20].

Porphyrins are π-conjugated macrocyclic systems with high chemical and thermal stability. The incorporation of the porphyrins into solid inorganic substrates enhances their ability to remove metal ions and improves their *ligand* binding *properties*[21]. Actually, the nitrogen atoms in the tetrapyrrole ring act as ligands and attract metal ions because of their strong electron-donor properties; thus, providing high removal efficiency via formation of metal–nitrogen coordination bonds[22]. In this work, we reported the synthesis and characterization of tetrakis(4-hydroxyphenyl)porphyrin incorporated into functionalized SBA-15 (THPP-SBA-15) (Scheme 1). Then, its performance in the adsorption of toxic heavy metal of Pb^{2+} from aqueous solution was investigated.

EXPERIMENTAL

Materials and Methods

Tetraethylorthosilicate (TEOS), pluronic P123 (tri-block copolymer $EO_{20}PO_{70}EO_{20}$) and (3-chloropropyl) trimethoxysilane (CPTMS), were purchased from Aldrich Co. Pure analytical pyrrole, 4-hydroxybenzaldehyde and propionic acid were supplied from Merck Co. All solvents used in this work were purchased from Merck Co. and used without further purification.

The morphology of SBA-15, CPTMS-SBA-15 and THPP-SBA-15 was examined using a Tescan (model Vega II) Scanning Electron Microscope (SEM). Powder X-ray Diffraction (XRD) was carried out using a Philips (Xpert MPD) diffractometer. Fourier transform infrared (FT-IR) spectra were recorded on a Shimadzu-8400S spectrometer in the range of 400-4000 cm^{-1} using KBr pellets. Diffuse Reflectance Spectra (DRS) were prepared via a Shimadzu (MPC-2200) spectrophotometer. The UV-Vis absorption study was performed at room temperature in the wavelength range of 190-800 nm on a UV-Vis spectrometer (ShimadzuUV-1700). Surface area and pore size distribution were determined using Brunauer–Emmett–Teller (BET) multilayer nitrogen adsorption method in a conventional volumetric technique by ASAP 2020 micromeritics instrument. The concentration of metal ions was measured by using an inductively coupled plasma spectrometer (ICP-AES, Shimadzu, model ICPS – 700, ver. 2).

Synthesis of SBA-15 modified with (3-chloropropyl)triethoxysilane (CPTMS-SBA-15)

Mesoporous silica SBA-15 material was prepared using TEOS as silica precursor and P123 as template via the hydrothermal method [23]. P123 (4 g) was dissolved in 100 mL HCl (2.1 M); the solution was stirred at 40°C for duration of 4 h. Then, TEOS (6.3 g) was slowly added to the solution and the water-P123 mixture was kept under static conditions at 40°C for duration of 24h. The resulting gel was crystallized by hydrothermal treatment at 100°C for 48h in a Teflon autoclave. Next, the resulting white solid was filtered and washed with deionized water several times, air-dried at room temperature and calcined at 550°C to remove the surfactant template for duration of 5h.

The surface modification of SBA-15 was carried out: 2.8 mL of CPTMS was added dropwise to 0.4g of SBA-15 suspended in 25mL of anhydrous toluene. Then, the reaction mixture has refluxed in a round bottom flask at 110 °C for duration of 24 h. The resulting precipitate was filtered, washed with toluene and ethanol, and dried overnight at 100°C. The sample is designated as CPTMS-SBA-15.

Synthesis of tetrakis(4-hydroxyphenyl)porphyrin (THPP)

0.52 mL of newly distilled pyrrole was added to a round-bottom ûask containing 4-Hydroxy benzaldehyde (915mg) dissolved in 40mL propionic acid. The mixture was refluxed for duration of 1 h; then, 50 mL EthOH was added. The mixture was cooled to room temperature and placed in an ice bath for duration of 60 min. The separated product was ûltered off and washed several times with the mixture of propionic acid and EthOH (1:1), and chloroform, respectively. The resulting product was purified via column chromatography.

Synthesis of THPP-SBA-15 hybrid

20 mL NaOH (0.05M) was added to 0.026 g THPP dissolved in 30mL DMF and stirred for 10 min. The resulting solution was added to a round bottom flask containing 0.3 g CPTMS-SBA-15 dispersed in 10 mL DMF. Then, the reaction mixture was heated with stirring at 70°C for duration of 24h. The resulting precipitate was filtered, washed with DMF three times and air-dried at room temperature. *To neutralize the resulting red powder, it was treated with* HCl 5% solution to reach a green color. After filtration, the product was washed thoroughly with deionized water. Finally, this green solid dried at 90°C for duration of 10h and henceforth denoted as THPP-SBA-15.

Heavy metal adsorption experiments

Lead nitrate was dissolved in deionized water to prepare initial metal ion solutions with concentrations of 10 mg/L, 20 mg/L, 50 mg/L, 80 mg/L, 100 mg/L, and 200 mg/L. 0.008 mg of adsorbent and 10 mL of metal ion solutions were placed in stoppered vials and stirred (at the rate of 300 rpm) for 100 min at room temperature. The resulting mixtures were filtered to collect the final solutions. The metal concentration of the initial and final solutions was determined via ICP-AES spectroscopy.

RESULTS AND DISCUSSION

Characterization

X-ray powder diffraction (XRD)

The low-angle XRD spectra for SBA-15, CPTMS-SBA-15 and THPP-SBA-15 are shown in Fig. 1. All three synthesized materials exhibited three well-resolved diffraction peaks including a strong peak at 2è of 1.09 corresponding the distance between two successive walls (that is, one pore diameter plus a wall thickness) and two peaks at 2è of 1.57 and 1.8, which are characteristic of a well-ordered SBA-15 type material. The intensities

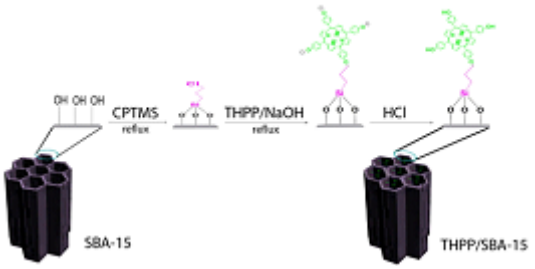

Scheme 1: Schematic presentation of THPP-SBA-15 synthesis from SBA-15

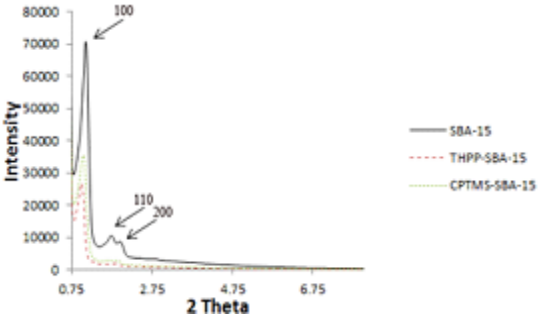

Fig. 1: XRD plot of SBA-15, CPTMS-SBA-15 and THPP-SBA-15

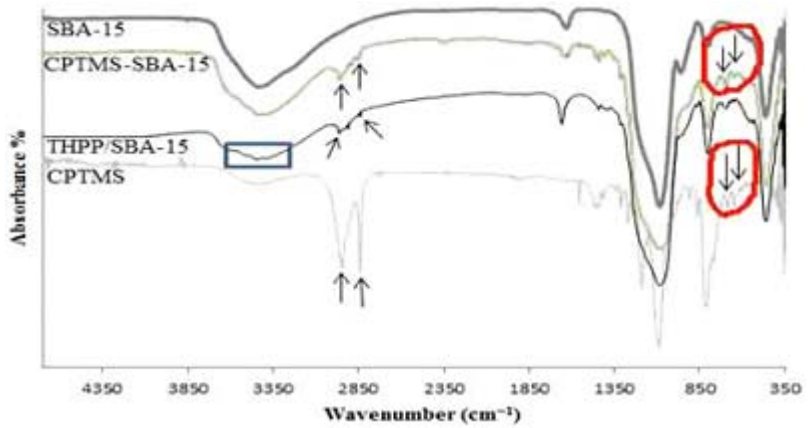

Fig. 2: FT-IR spectra of SBA-15, CPTMS-SBA-15 and THPP-SBA-15

of the XRD peaks for CPTMS-SBA-15 and porphyrin-SBA-15 are substantially lower than those measured for SBA-15, which is probably caused by a slight alteration of the mesoporous structure ordering that likely results from distribution of organic groups throughout the SBA-15 mesoporous silica. Thereby, these results prove the evidence that functionalization occurred mainly inside the mesoporous channels.

FT-IR spectra

Fig.2 shows the infrared spectra of SBA-15, CPTMS-SBA-15, and porphyrin-SBA-15. In the infrared spectrum of SBA-15, the bands 811 and 1087 cm^{-1} belong to the symmetric and asymmetric stretching vibrations of the Si–O–Si bond. The bands of 463 and 967cm^{-1} have been assigned to the torsion vibration of the Si–O–Si bond and the stretching vibration of the silanol's groups (Si–OH),

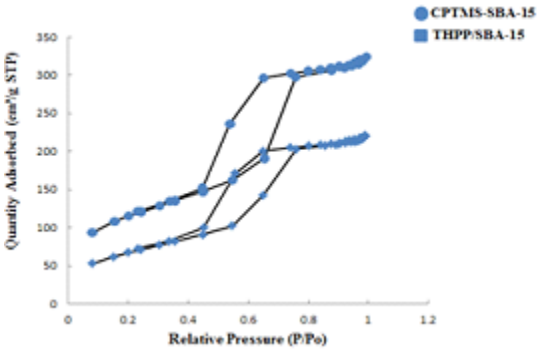

Fig. 3(A): Nitrogen adsorption-desorption isotherms of CPTMS-SBA-15 and THPP-SBA-15

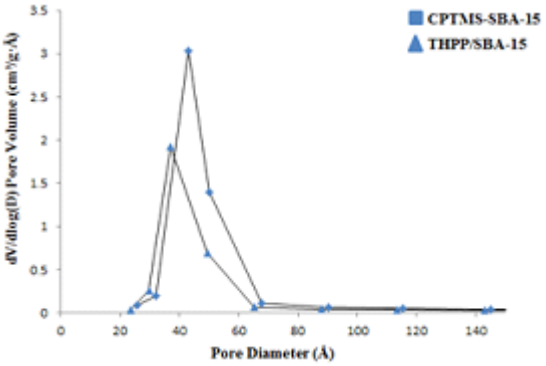

Fig. 3(B): Pore distribution of CPTMS-SBA-15 and THPP-SBA-15

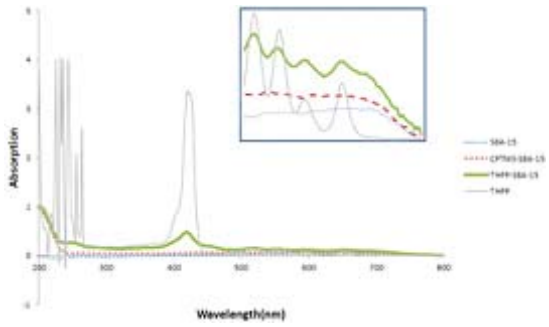

Fig. 4: The UV-Vis spectra of SBA-15, CPTMS-SBA-15, THPP-SBA-15 and THPP

respectively. The broad peak of 3000-3467cm^{-1} is associated with stretching vibrations of superficial silanol groups (Si–OH)[24]. In the CPTMS-SBA-15 spectrum, the peaks observed at around 2926, 2847, 1463, and 722cm^{-1} are related to asymmetric stretching, symmetric stretching, bending vibrations of aliphatic C–H bonds, and the vibration of Si–C bonds, respectively. In addition, successful incorporation of the chloropropyl group into the SBA-15 mesoporous material's network can be confirmed from the peak near 595cm^{-1}, due to presence of stretching vibrations of C-Cl bond [25]. In the THPP-

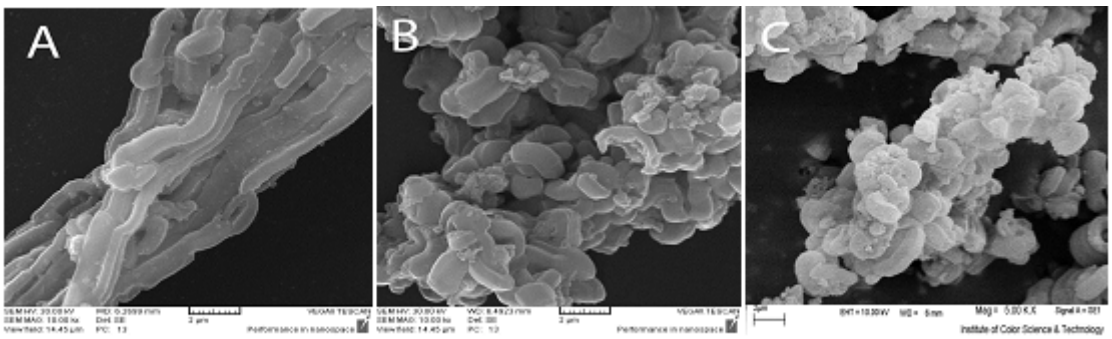

Fig. 5: The SEM images of (A) SBA-15, (B) CPTMS-SBA-15 and (C) THPP-SBA-15

SBA-15 spectra, strong band was observed about 3394 cm^{-1} that assigned to the overlapped O-H stretching vibration with N-H (pyrrole) vibration. In the spectrums of SBA-15, CPTMS-SBA-15 and THPP-SBA-15 There is a peak about 1630 cm^{-1} that relates to bending vibrations of adsorbed water.

Nitrogen adsorption-desorption

The nitrogen adsorption-desorption analysis was performed at 77 K. Adsorption-desorption isotherms for CPTMS-SBA-15 and THPP-SBA-15 are shown in Fig 3-A. The corresponding isotherms show type IV isotherm in the IUPAC classiûcation that reveal well-ordered mesoporous materials.

The actual pore radius, r_p, should be rewritten as:

$$r_p = r_k + t$$

where t represents the thickness of the adsorbed layer on the surface.

Accocding to the BJH theory the weighted average pore diameter is calculated as follows:

$$D_{avg\ k} = \frac{(2)(R_{Ck} + R_{Ck+1})(R_{Ck})(R_{Ck+1})}{{R_{Ck}}^2 + {R_{Ck+1}}^2}$$

Where $D_{avg\ k}$ is the diameter of a pore which would have a surface area that is the average of the areas for pore radius R_{Ck} and R_{Ck+1}, if its length was the mean of the lengths at those radii.

The following results have been arisen from BET and BJH method[26,27]. The BET surface area of THPP-SBA-15 is 249 m^2/g, which is lower than that of CPTMS-SBA-15 (414 m^2/g), and the average pore size is decreased from 54 Å for CPTMS-SBA-15 to 48 Å for THPP-SBA-15. These results indicate that the void pores of CPTMS-SBA-15 have been occupied by THPP and SBA-15 material and show general modiûcation due to presence of organic moieties. Generally, the modified adsorbents have a lower surface area and pore size than the unmodified ones[28]. Pore size distribution curves for CPTMS-SBA-15 and THPP-

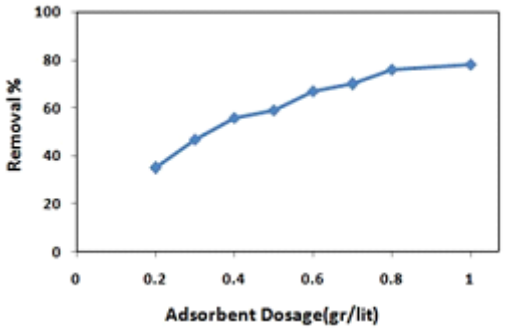

Fig. 6: Effect of the dosage on the removal of Pb^{2+} ions by THPP-SBA-15

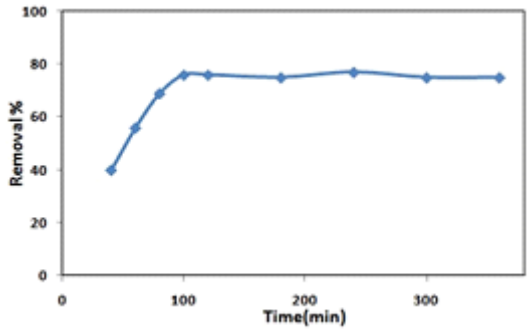

Fig. 7: Effect of the contacting time on the removal of Pb^{2+} ions by THPP-SBA-15

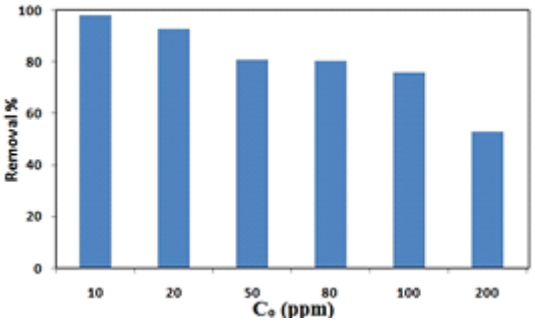

Fig. 8: Effect of initial concentration on the removal of Pb^{2+} ions by THPP-SBA-15

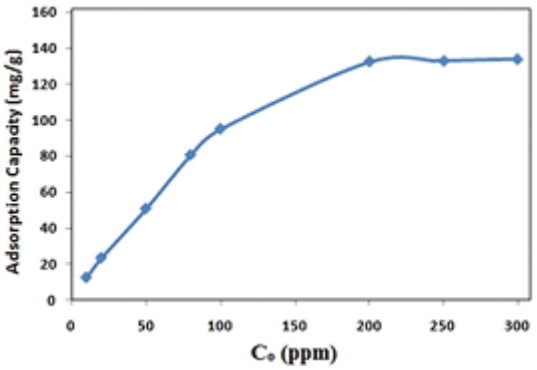

Fig. 9: Adsorption isotherm of Pb^{2+} ions on THPP-SBA-15

SBA-15 are shown in Fig 3-B. Both of them reveal a narrow pore size distribution with the maximum pore diameter of the distribution curve around 43 and 37 Å for CPTMS-SBA-15 and THPP-SBA-15, respectively.

UV-Vis spectroscopy

The UV-Vis absorption spectra of the pure THPP, SBA-15, CPTMS-SBA-15, and the THPP-SBA-15 are shown in Fig. 4. The UV–vis absorption spectrum of pure THPP shows absorption around 400 nm (the soret band), followed by several weaker absorptions (Q bands) at higher wavelengths (500–700 nm). In the same regions in the UV-Vis spectra of SBA-15 and CPTMS-SBA-15, no absorption peaks related to porphyrin are observed. While in the THPP-SBA-15 spectrum, the soret band and the Q bands are similar to the spectrum of pure THPP, but the soret band of the THPP incorporated into SBA-15 is red-shifted. The intension of this peak decreased and encapsulation of THPP by SBA-15 may cause lowering this intention because porphyrin is now surrounded by interior surface of SBA-15.

Morphology of materials

Fig.5-A shows a SEM image of the SBA-15 with rod-like structure that it's directions are parallel to a long axis, while Fig.5-B and 5-C show images of modified SBA-15 with CPTMS and porphyrin, respectively. In comparison to pure SBA-15, the mentioned materials display typical fibrous type morphologies (as usually seen in the SBA-15 materials) and shorter channel lengths, while general morphological properties of these silica materials indicate no changes after the modification process.

Adsorption behavior of THPP-SBA-15

Measurements were based on 100mL solution with initial Pb^{2+} ion concentration of 100 mg/L. The adsorption efficiency of Pb^{2+} as a function of adsorbent dosage is presented in Fig. 6. It is observed that the removal efficiency increases as the adsorbent dosage is raised. When a dosage of 0.8 g/L is used, the removal efficiency reaches 80%, indicating that the adsorbent shows strong affinity to Pb^{2+}. In considering the removal efficiency, an adsorption dosage of 0.8 g/L is selected for the following studies.

To determine an optimum contact time between the THPP-SBA-15 and lead ion solutions, adsorption efficiency of metal ion was measured as a function of contact time and the results are presented in Fig. 7. As shown in this figure, the maximum removal of lead ions attained within duration of 100 min. In order to interpret the kinetic characteristics of metal adsorption processes, a pseudo second order equation model can be used to evaluate experimental data.

The effect of initial concentrations on metal ion adsorption was investigated by varying the initial concentrations of the metal ion during100 min of equilibration time. The effect of initial concentration on the removal of Pb^{2+} ions by THPP-SBA-15 is presented in Fig. 8.

Adsorption isotherm is studied to determine the adsorption behavior of an adsorbent. The capacities of THPP-SBA-15 to adsorb Pb^{2+} are investigated by measuring the initial and final concentration of metal ion. Fig. 9 shows the adsorption isotherm for the adsorbent. Isotherm curves demonstrate adsorption as a function of the equilibrium concentration of metal ion in solutions. This figure shows that adsorption of the metal ions enhances with increase in ion concentrations and inclines to achieve saturation point at higher concentrations. This increase in loading capacity of the adsorbent with relation to the metal ions concentration can be explained with the high driving force for mass transfer. The Langmuir adsorption isotherm equation was used to normalize the adsorption data. The general form of the Langmuir isotherm equation is as follows:

$$\frac{q_e a_L}{K_L} = \frac{K_L C_e}{(1 + K_L C_e)}$$

where C_e is the equilibrium concentration of Pb^{2+} in the solution (mg/L), q_e is the amount of metal ion adsorbed per unit of adsorbent at equilibrium (mg/g) and a_L (L/mg) and K_L (L/g) are the Langmuir constants. In addition, the maximum adsorption capacity (mg/g) is indicated by $[Q_m = K_L/a_L]$. As q_{max} depends on the number and structure of adsorption sites, as long as there are unoccupied sites, the adsorption process will increase with

increasing metal ion concentrations, but as soon as all of the sites are occupied, a further increase in concentrations of metal ion solutions does not increase the amount of Pb^{2+} on adsorbents. This Eq. can be rearranged into linear form:

$$\frac{C_e}{q_e} = C_e(\frac{a_L}{K_L}) + (\frac{1}{K_L})$$

The values of a_L and K_L are calculated from the slope and intercept of the plot of C_e/q_e vs. C_e. The amount of Pb^{2+} adsorbed (mg/g) is calculated be the following equation:

$$q_e = \frac{V(Ci - Cf)}{m}$$

where C_i and C_f are the initial and final concentrations of Pb^{2+} in mg/L, respectively; V is the volume of experimental solution in l, and m is the weight of THPP-SBA-15 in g. Results show that the maximum adsorption capacity (q_{max}) for the adsorption of Pb^{2+}onto THPP-SBA-15 is found to be 134 mg/g.

CONCLUSION

In this study, a new adsorbent for heavy metal removal from aqueous media was successfully prepared. Such an adsorbent has a mesoporous structure with large surface area and pore volume. These features make it an effective and convenient adsorbent for heavy metal removal. The adsorption process fitted well with Langmuir isotherm and its kinetics abides the pseudo second order kinetic equation. In conclusion, the porphyrin functionalized mesoporous silica is a promising adsorbent for heavy metal removal from water sources such as river water, lake water, groundwater, and tap water.

REFERENCES

1. Guo X, Fu L, Zhang H, Carlos LD, Peng C, Guo J, Yu J, Deng R, Sun L. *New J. Chem.* **2005**, 29 (10):1351-1358.
2. Yan B, Li Y-Y, Qiao X-F. *Microporous Mesoporous Mater.* **2012**, 158 (0):129-136.
3. Bartl MH, Scott BJ, Huang HC, Wirnsberger G, Popitsch A, Chmelka BF, Stucky GD. *Chem. Commun.* **2002**, (21):2474-2475.
4. Zhang W-H, Shi J-L, Wang L-Z, Yan D-S., *Chem. Mater.* **2000,** 12 (5):1408-1413.
5. Zhao D, Sun J, Li Q, Stucky GD. *Chem. Mater.* **2000**, 12 (2):275-279.
6. JavadKalbasi R, Massah A, Zamani F, Bain A, Berno B. *J. Porous Mater.* **2011**, 18 (4):475-482.
7. Scott BJ, Wirnsberger G, Stucky GD. *Chem. Mater.* **2001**, 13 (10):3140-3150.
8. Madhugiri S, Dalton A, Gutierrez J, Ferraris JP, Balkus KJ. *J. Am. Chem. Soc.* **2003**, 125 (47):14531-14538.
9. Kalbasi RJ, Kolahdoozan M, Rezaei M. *Mater. Chem. Phys.* **2011**, 125 (3):784-790.
10. Kucœtrowski P, Chmielarz L, Dziembaj R, Cool P, Vansant EF. *J. Phys. Chem. B.* **2005**, 109 (23):11552-11558.
11. Chen Z, Zhou L, Zhang F, Yu C, Wei Z. *Appl. Surf. Sci.* **2012**, 258 (13):5291-5298.
12. Huber C, Moller K, Bein T. *Journal of the Chemical Society, Chem. Commun.* **1994**, (22):2619-2620.
13. Takahashi H, Li B, Sasaki T, Miyazaki C, Kajino T, Inagaki S. *Microporous Mesoporous Mater.* **2001**, 44–45 (0):755-762.
14. Liu AM, Hidajat K, Kawi S, Zhao DY. *Chem. Commun.* **2000**, (13):1145-1146.
15. Joseph T, Deshpande SS, Halligudi SB, Vinu A, Ernst S, Hartmann M. *J. Mol. Catal. Chem.* **2003**, 206 (1–2):13-21.
16. Yang H, Xu R, Xue X, Li F, Li G. *J. Hazard. Mater.* **2008**, 152 (2):690-698.
17. Xia K, Ferguson RZ, Losier M, Tchoukanova N, Brüning R, Djaoued Y. J. Hazard. Mater. **2010**, 183 (1–3):554-564.
18. Li G, Zhao Z, Liu J, Jiang G. *J. Hazard. Mater.* **2011**, 192 (1):277-283.
19. Bai L, Hu H, Fu W, Wan J, Cheng X, Zhuge L,

Xiong L, Chen Q. *J. Hazard. Mater.* **2011**, 195 (0):261-275.
20. Aguado J, Arsuaga JM, Arencibia A, Lindo M, Gascón V. *J. Hazard. Mater.* **2009**, 163 (1):213-221.
21. Thomas DW, Martell AE. J. Am. Chem. Soc. **1959**, 81 (19):5111-5119.
22. Jeong E-Y, Ansari MB, Mo Y-H, Park S-E. J. Hazard. Mater. **2011**, 185 (2–3):1311-1317.
23. Zhao D, Huo Q, Feng J, Chmelka BF, Stucky GD. J. Am. Chem. Soc. **1998**, 120 (24):6024-6036.
24. Maurya MR, Chandrakar AK, Chand S. J. Mol. Catal. A: Chem. **2007**, 270 (1–2):225-235.
25. Silverstein RM, Bassler GC, Morrill TC, Spectrometric identification of organic compounds, John Wiley and Sons, New York, fourth ed. Edn, (1981).
26. Brunauer S, Emmett PH, Teller E. *J. Am. Chem. Soc.* **1938**, 60 (2):309-319.
27. Barrett EP, Joyner LG, Halenda PP. *J. Am. Chem. Soc.* **1951,** 73, (1):373-380.
28. Zimowska M, Michalik-Zym A, Po³towicz J, Bazarnik M, Bahranowski K, Serwicka EM. *Catal. Today.* **2007,** 124, (1–2):55-60.
29. Shakiba Nahad M, Mohammadi Ziarani Gh, *Orient. J. Chem.* **2013,** 29, (4):1597-1603.
30. Giraldo L, Gonzales Navarro M F, Moreno Pirajan J C, *Orient. J. Chem.* **2013**, 29, (4): 1297-1309.